Blackbody Spectrum Revisited in the Near Field

Arthur Babuty,[1] Karl Joulain,[2,*] Pierre-Olivier Chapuis,[3,4] Jean-Jacques Greffet,[5] and Yannick De Wilde[1,†]

[1]*Institut Langevin, ESPCI ParisTech, CNRS, 75238 Paris Cedex 05, France*
[2]*Institut P', CNRS, Université de Poitiers, 86022 Poitiers, France*
[3]*Catalan Institute of Nanotechnology (ICN), Campus UAB, 08193 Bellaterra, Spain*
[4]*Centre de Thermique de Lyon (CETHIL), CNRS, INSA Lyon, UCBL, 69621 Villeurbanne, France*
[5]*Laboratoire Charles Fabry, Institut d'Optique, CNRS, Université Paris-Sud, 91127 Palaiseau, France*
(Received 14 February 2012; revised manuscript received 23 February 2013; published 5 April 2013)

We report local spectra of the near-field thermal emission recorded by a Fourier transform infrared spectrometer, using a tungsten tip as a local scatterer coupling the near-field thermal emission to the far field. Spectra recorded on silicon carbide and silicon dioxide exhibit temporal coherence due to thermally excited surface waves. Finally, we evaluate the ability of this spectroscopy to probe the frequency dependence of the electromagnetic local density of states.

DOI: 10.1103/PhysRevLett.110.146103 PACS numbers: 68.37.Uv, 44.40.+a

Near-field optical measurements can probe the spectral properties of materials with a subwavelength resolution [1–4]. The near-field interaction between the sample and the probe may result in frequency shifts and broadening of plasmonic resonances [5,6]. Recent techniques [7,8] based on the detection of the mechanical movement of the tip appear to be sensitive and free of frequency shift. In this Letter, we use a near-field microscope to probe the spectrum of the thermally emitted radiation instead of studying the optical properties of the material. Our motivations to study the spectrum of the thermally emitted field are manifolds. It has been predicted [9,10] that the spectra are very different in the far field and in the near field. In particular, it was predicted [9] that the intensity increases by orders of magnitude and becomes quasimonochromatic when surface waves are supported by the interface. The increase of the near-field intensity has been observed experimentally [11]. As the energy emitted by a surface is much larger close to the surface, the energy flux between two surfaces at different temperatures separated by a submicron distance is also enhanced by orders of magnitude [12,13]. This has been reported in several recent papers [14–16] where the enhancement due to the excitation of surface waves on glass was observed. However, while the enhancement of the energy density in the near field due to the excitation of surface phonon polaritons appears to be well documented, its spectrum has not been studied yet. The prediction [9] of a quasimonochromatic spectrum could find applications. It has been predicted that the efficiency of a thermophotovoltaic device could be improved in the near field [17–19]. Another application based on the quasimonochromatic character of the thermal field is the design of a thermal rectifier [20].

So far, there is only one experimental observation of the spectrum of the thermal emission close to the surface [21] obtained using a heated tip brought in contact with a surface under study. In this experiment, the sample is heated by the hot tip and is therefore not at thermal equilibrium. In our experiment, we aim at placing the system in thermodynamic equilibrium by bringing the sample at uniform temperature. As a consequence, we consider the reverse situation of a homogeneously heated surface, which we achieve by heating the entire sample using a heated sample holder [11]. Hence, we make sure that all the electromagnetic surface modes are equally populated according to the Bose-Einstein statistics. It follows that the emitted electromagnetic energy density is proportional to the electromagnetic local density of states (EM-LDOS) as discussed in Ref. [22]. This quantity plays a fundamental role not only in the thermodynamic properties of the system but also when studying the decay rate of an emitter. Indeed, Fermi golden rule states that the decay rate is proportional to the number of final states available. Hence, the LDOS can be derived from decay rate measurements [23–27]. Note that the LDOS projected parallel to the dipole axis is detected when doing these measurements. However, the spectral and polarization dependence can be factorized to a large extent. Indeed, we are interested in the spectral dependence due to the presence of a surface wave. We stress that one should avoid heating of a too small area of the sample when investigating surface polaritons as their spatial coherence can extend up to several tens of wavelengths [28,29].

Here, we report spectral measurements of the intensity in the near field. We use a scattering type near-field microscope that scatters the near-field intensity into the far field. In what follows, we first describe the experimental setup and present the data. We then discuss the results and introduce a simple model to account for the perturbation due to the tip.

The experimental setup is presented in Fig. 1. A resistive heater controls the temperature T of the sample up to 473 K in order to populate the modes by thermal excitation. To detect the thermally excited modes, we use a tungsten tip

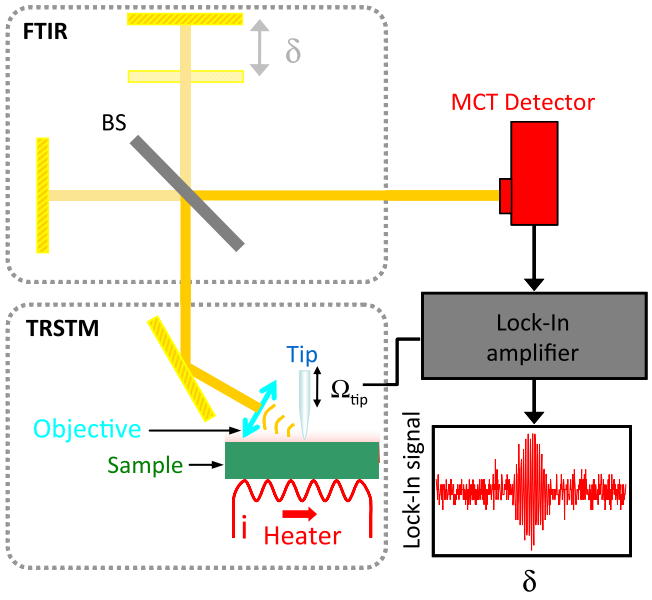

FIG. 1 (color online). Sketch of the near-field thermal photon spectroscopy setup. A resistive heater allows raising the sample temperature up to 473 K. Thermal emission is scattered in the near field by the apex of a tungsten tip which oscillates in intermittent contact, with a fixed amplitude ~100 nm and frequency $\Omega \approx 32$ kHz, perpendicularly to the sample surface. The scattered electromagnetic field is collected sideways with a Cassegrain objective (Numerical aperture NA = 0.5) and analyzed by a FTIR combined with a MCT detector. The intensity at the detector is measured at Ω or at 2Ω with a lock-in amplifier in order to eliminate background radiation, while the FTIR operates in step-scan mode. The spectrum of the intensity of the NFTE scattered by the tip $S_{\mathrm{exp}}(\sigma)$, where σ is the wave number, is obtained after a Fourier transform of the interferogram [30].

that acts as a scatterer coupling the near field to the far field. The tip oscillates perpendicularly to the sample surface at a frequency Ω and hits it periodically. An electronic feedback maintains its averaged height at a preset value. The scattered field is collected sideways by a Cassegrain objective mounted on a commercial infrared microscope, and guided towards a nitrogen cooled mercury cadmium telluride (MCT) detector through a Fourier transform infrared spectrometer (FTIR). A lock-in amplifier connected to the output of the detector allows one to detect the signal at Ω or at a higher harmonic. Note that it has been shown in Ref. [11] that the detected signal, obtained thanks to the setup which has been called thermal radiation scanning tunneling microscopy (TRSTM), is not due to modulation of the sample temperature by the tip, and that it survives when the tip is close even if not in intermittent contact with the sample surface. The FTIR includes a Michelson interferometer. A beam splitter separates the incoming radiation into two beams which interfere at the detector after being reflected. The FTIR is operated in step scan, changing the path difference δ between the two beams step by step with moving mirrors. A stabilization delay of five times the time constant of the lock-in amplifier is set at each step before recording the signal S from the lock-in. The curve $S_{\mathrm{exp}}(\delta)$ constitutes the interferogram. The spectrum of the incoming radiation $S_{\mathrm{exp}}(\sigma)$, where σ is the wave number ($\sigma = 1/\lambda$, with λ the wavelength), is obtained by a Fourier transform of $S_{\mathrm{exp}}(\delta)$ as in standard FTIR measurements [30].

To demonstrate the efficiency of TRSTM spectroscopy, we present in Figs. 2(a) and 2(b), the near-field thermal emission (NFTE) spectra recorded above planar silicon carbide (SiC) and silicon dioxide (SiO_2) surfaces. Both materials support surface phonon polaritons, which are

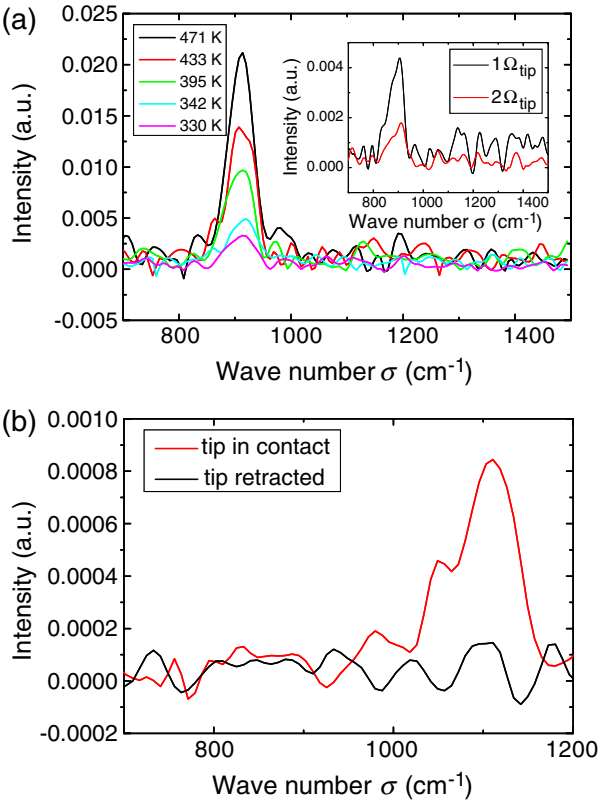

FIG. 2 (color online). Experimental near-field thermal photon spectra. (a) Spectra of the NFTE detected on silicon carbide (SiC) at various temperatures between 471 and 330 K when demodulating the signal at the tip oscillation frequency Ω showing a peak due to thermally excited surface phonon polaritons. Inset: Same measurement at $T = 473$ K, when demodulating the signal either at Ω or at 2Ω to demonstrate that the signal is due to scattering of the NFTE by the tip apex. (b) Spectra of the NFTE detected on silicon dioxide (SiO_2) showing that the contribution due to surface phonon polaritons when the tip is at the surface disappears when it is withdrawn by 1 μm. The resolution in the spectra is 6 cm^{-1}. The near-field thermal photon spectra measure the frequency dependence of the electromagnetic local density of states (EM-LDOS) at the tip apex. The experimental spectra measured with the tip on SiC and SiO_2 exhibit pronounced peaks associated with surface phonon polaritons, which directly demonstrates partial temporal coherence of thermal emission in the near field of both materials, in striking contrast with far-field blackbody radiation [9,10,22].

expected to produce a sharp peak in the EM-LDOS spectra at $\sigma_{\text{th}} = 948\ \text{cm}^{-1}$ for SiC and $\sigma_{\text{th}} = 1156\ \text{cm}^{-1}$ for SiO_2 [9,10,22], and spatial coherence of NFTE has been demonstrated on a SiC sample using a diffraction grating at its surface [28]. The measured near-field spectra exhibit peaks at $\sigma_{\text{exp}} = 913\ \text{cm}^{-1}$ for SiC and $\sigma_{\text{exp}} = 1110\ \text{cm}^{-1}$ for SiO_2. This is in good agreement with the theoretical values, despite a slight redshift of about 40 cm^{-1} which is systematically observed in the experiments with respect to theory. These spectra are the experimental demonstration of partial temporal coherence of thermal emission in the near field, a behavior predicted more than a decade ago [9].

In the experiments, NFTE scattered at frequency Ω is separated from far-field thermal emission background using a lock-in amplifier. Most importantly, we showed that the spectrum recorded with the signal detected at 2Ω exhibits a peak as the one observed at Ω [Fig. 2(a), inset]. The field detected is thus strongly nonlinear with the distance on the scale of the tip oscillation amplitude, typically 100 nm [11]. We thus verify that the main part of the signal arises from tip apex scattering, and not from the slowly varying far-field background scattered by the oscillating tip support. The peak absence when withdrawing the tip by 1 μm [Fig. 2(b)] further confirms the near-field signal origin. Another important verification aims at proving that measured spectra are not due to room temperature blackbody radiation produced by the environment and scattered by the tip. Measuring the SiC sample spectra between 473 and 330 K, we clearly observe that the peak intensity decreases with temperature [Fig. 2(a)], as expected for electromagnetic surface modes which are thermally excited. The temperature dependence of the dielectric constant is such that the linewidth of the EM-LDOS is expected to vary by a few cm^{-1} within this range [29]. We could not resolve this thermal effect because the tip-sample interaction induces a broadening of the EM-LDOS peaks of a few tens of cm^{-1}, as we discuss later. Neither did we detect in the spectra the influence of the pressure which intermittently increases in the material when the tip hits its surface, with a duty cycle of a few percent. Remarkably, the experimental spectra presented in Fig. 2 don't show any features related to the far-field thermal emission scattered by the tip since the signal demodulation at Ω and 2Ω efficiently suppresses the far-field components of the thermal field which exhibit slow variations in the direction perpendicular to the sample surface [31]. Note that we have also verified that the thermal emission from the tip itself contributes negligibly to the spectra recorded in our experimental configuration (see the Supplemental Material, Part B [32]).

As pointed out previously, the peaks observed are redshifted. Similar frequency shifts have been observed in experiments with scattering type probes combined with an external source, which probe the tip-sample interaction, and explained using a quasielectrostatic model [3,5]. Local spectroscopy probes which detect a mechanical response of an atomic force microscope cantilever due to absorption, don't produce any shift [6,7], but they have not been adapted yet to the detection of the NFTE. In order to explain the shifts, we developed a full theoretical description of a dipolar tip interacting with a plane surface, including retardation effects [33]. The tip is approximated by a point dipole located at its center. Note that the dipole model has been established for the qualitative description of apertureless near-field optical scanning microscopy [34], which yields valuable physical insights into the tip-sample coupling such as spectral shifts. This approach neglects thus the anisotropic response of the tip with respect to scattering [35], but appears to be sufficient to describe the experimental spectra, as shown below. The electromagnetic field $\boldsymbol{E}_d$ received at a detector includes two contributions: one direct dipolar field and another one due to the reflection by the sample (see Fig. 3). The electric dipole moment at the tip position $\boldsymbol{r}_t$ is the product of the tip polarizability α^E with the local field at the tip position $\boldsymbol{E}_{\text{local}}(\boldsymbol{r}_t)$. The field above the surface in the absence of the tip is denoted $\boldsymbol{E}_0(\boldsymbol{r}_t)$. In order to account for the multiple reflections between the dipolar tip and the sample [see Fig. 3(a)], we introduce an effective polarizability so that $\alpha^E \boldsymbol{E}_{\text{local}}(\boldsymbol{r}_t) = \vec{\boldsymbol{\alpha}}^E_{\text{eff}} \boldsymbol{E}_0(\boldsymbol{r}_t)$. It can be simply expressed with the help of $\vec{\boldsymbol{G}}^R_{EE}(\boldsymbol{r}_t, \boldsymbol{r}_t)$, the reflected Green tensor giving the field at the tip position from an elementary dipole at the tip position:

$$\vec{\boldsymbol{\alpha}}^E_{\text{eff}} = \alpha^E [\vec{\boldsymbol{I}} - \alpha^E \vec{\boldsymbol{G}}^R_{EE}(\boldsymbol{r}_t, \boldsymbol{r}_t)]^{-1}.$$

The expression of $\vec{\boldsymbol{\alpha}}^E_{\text{eff}}$ is an extension beyond the quasielectrostatic approximation which has previously been used to describe scattering tips [3,34]. Finally, the field at the detector position can be cast in the form

$$\boldsymbol{E}_d = (\vec{\boldsymbol{g}} + \vec{\boldsymbol{g}}_r) \vec{\boldsymbol{\alpha}}^E_{\text{eff}} \boldsymbol{E}_0,$$

where $\vec{\boldsymbol{g}}$ and $\vec{\boldsymbol{g}}_r$ are classical far-field operators relating the dipole at a point to the field at another point in the far field approximation, and, respectively, describing the direct propagation and the one including reflection at the surface. The signal $\langle S_{\text{th}}(\sigma) \rangle$ at a detector subtending an elementary solid angle $d\Omega$ is proportional to

$$\langle S_{\text{th}}(\sigma) \rangle = \frac{\varepsilon_0 c}{2} |\boldsymbol{E}_d|^2 r_d^2 d\Omega,$$

where r_d is the tip-detector distance. This expression contains quadratic expressions of $\boldsymbol{E}_0$ and $\vec{\boldsymbol{\alpha}}^E_{\text{eff}}$. The quadratic expressions $\langle \boldsymbol{E}_0(\boldsymbol{r}_t) \boldsymbol{E}_0(\boldsymbol{r}_t) \rangle$ provide the electric component of the EM-LDOS, which is proportional to the Green tensor $\vec{\boldsymbol{G}}^R_{EE}(\boldsymbol{r}_t, \boldsymbol{r}_t)$ imaginary part [10]. The effective polarizability also depends on this quantity. Note that we have only written the electric part, but analogous magnetic terms can also be required. As a consequence, $\langle S_{\text{th}}(\sigma) \rangle$ is related to the EM-LDOS, but not simply proportional to it due to tip-sample interactions. This is exemplified in Fig. 3(b),

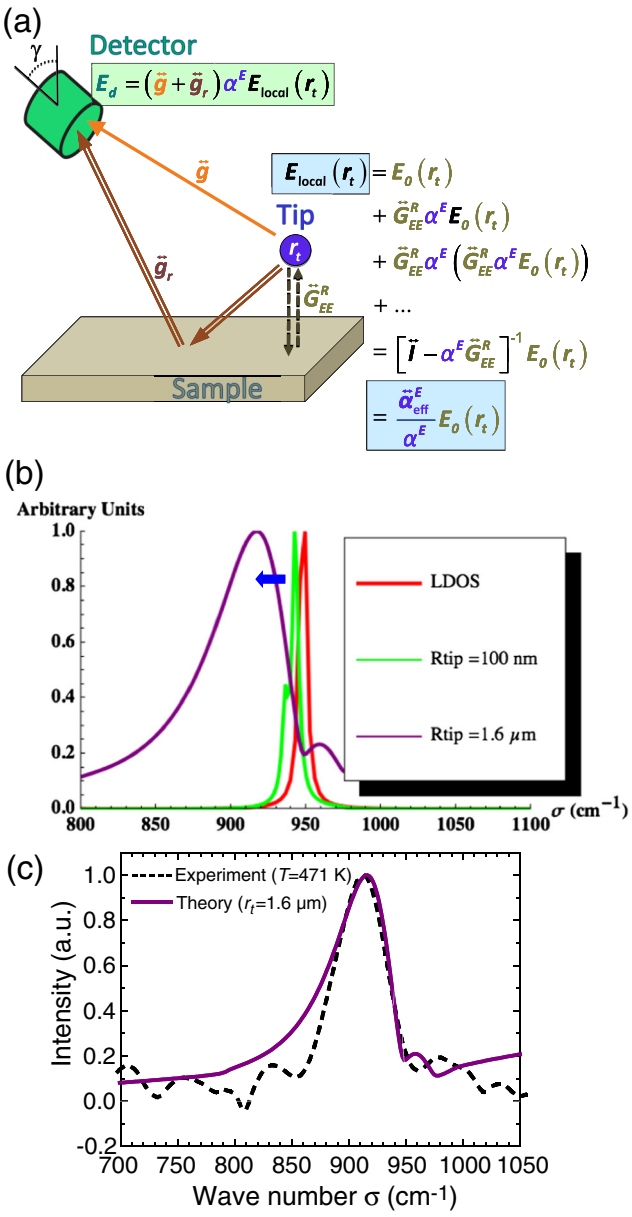

FIG. 3 (color online). The effect of the tip on the measured near-field thermal photon spectra. (a) The electromagnetic field scattered by the tip and reaching the detector can propagate through two different paths, being reflected by the sample before the detector or not. The local field at the tip position depends on multiple reflections with the sample, leading to a tip effective polarizability. (b) Computations of the electromagnetic local density of states (EM-LDOS) at $d = 100$ nm and simulation of the thermal radiation scanning tunnelling microscopy spectra TRSTM (σ) detected with tip radii $r_t = 100$ nm and $r_t = 1.6\,\mu$m for $d = r_t$. The TRSTM signal with $r_t = 1.6\ \mu$m is shifted and broadened due to the interaction between the sample and the tip. Note that the calculated TRSTM spectra have been divided here by $\theta(\omega, T) = \hbar\omega/[\exp(\hbar\omega/k_B T) - 1]$, where ω is the optical frequency, for a direct comparison with the EM-LDOS [9]. (c) Comparison between an experimental spectrum of the NFTE recorded on SiC at 471 K and a theoretical simulation with $r_t = 1.6\ \mu$m showing that both the redshift and the broadening are reproduced by the model.

where we compare the EM-LDOS calculated above SiC [9,10,22] with $\langle S_{\rm th}(\sigma)\rangle$ calculated for two spherical tip radii. Note that the detector is considered oriented at $\gamma = 30°$ with respect to the surface normal, in order to simulate the tilt angle of the Cassegrain objective in our setup. For the 100 nm radius, the peak in $\langle S_{\rm th}(\sigma)\rangle$ is close to that of the EM-LDOS. For larger tips, one expects larger differences between $\langle S_{\rm th}(\sigma)\rangle$ and the EM-LDOS. We found that an equivalent 1.6 μm-radius spherical tip fits very well the experimental spectra both above SiC and above SiO_2. We retrieve both peak frequency shifts (948 to 913 cm^{-1} for SiC, 1156 to 1110 cm^{-1} for SiO_2) and peak broadenings for the two materials tested. In comparison with the EM-LDOS, the signal detected in our experiment is thus shifted and broadened by the tip and its interaction with the sample which result in a frequency dependence in $\vec{\vec{\alpha}}^{E}_{\rm eff}$. As the spectra were measured with different tungsten tips prepared in a similar way, the fact that good fits are found when injecting the same tip radii in our model is an indication of the robustness of the method. Rather than representing the true geometry of the tip apex, it is reasonable to assume that the large value $r_t = 1.6\ \mu$m required to fit the spectra is linked to the peculiar geometry of the tip (see Supplemental Material [32]) which extends along the direction normal to the sample surface: a spherical dipole whose center is placed at r_t above the surface and the true extended tip scatterer produce similar spectra. The advantage of the spherical dipole model is that it requires only one fitting parameter, r_t, and that it can be solved exactly while including retardation effects. As shown in Fig. 3(b) and in the Supplemental Material (movie) [32], smaller tips such as the 100 nm radius one, should produce TRSTM spectra that are closer to the EM-LDOS ones. They could be obtained, for instance, by grafting a 100 nm radius metallic sphere at the extremity of a dielectric tip. As the signal-noise ratio in the spectra shown in Fig. 2 equals approximately 10, performing experiments with such a small scatterer requires the use of mid-infrared detectors with higher sensitivity than conventional MCT detectors and/or improvement of the efficiency of the collection optics. Note that the redshift in spectra measured with commercial AFM tips is smaller than with homemade tungsten tips, which points to a smaller effective dipole radius for this type of probes [21]. Our results demonstrate the efficiency of TRSTM spectroscopy as a means for local spectral characterization of materials, provided that they support surface resonances giving rise to a high electromagnetic energy concentration in the near field.

We have seen that TRSTM spectroscopy is a novel subwavelength spectroscopic method which allows us to probe the midinfrared spectrum of near-field thermal photons produced near room temperature. Similarly to fluorescent near-field probes based on decay rate measurements that have shown that spatial variations of the LDOS occur near plasmonic nanostructures [26,36], TRSTM spectroscopy

should allow for the investigation of spatial and spectral properties of the EM-LDOS of photonic and plasmonic nanostructures.

We thank R. Carminati and M. B. Raschke for discussions, F. Marquier for initial tests on FTIR, acknowledge support from the French National Research Agency (Grant No. ANR-07-NANO-039 "NanoFtir") and the Region Ile-de-France in the framework of C'Nano IdF (nanoscience competence center of Paris Region) for support. This work is supported by LABEX WIFI (Laboratory of Excellence within the French Program "Investments for the Future") under reference ANR-10-IDEX-0001-02 PSL*.

*To whom correspondence should be addressed.
karl.joulain@univ-poitiers.fr

†To whom correspondence should be addressed.
yannick.dewilde@espci.fr

[1] A. Hartschuh, E. J. Sanchez, X. S. Xie, and L. Novotny, Phys. Rev. Lett. **90**, 095503 (2003).
[2] M. Brehm, A. Schliesser, and F. Keilmann, Opt. Express **14**, 11 222 (2006).
[3] F. Huth, M. Schnell, J. Wittborn, N. Ocelic, and R. Hillenbrand, Nat. Mater. **10**, 352 (2011).
[4] L. Aigouy, F. X. Andreani, A. C. Boccara, J. C. Rivoal, J. A. Porto, R. Carminati, J.-J. Greffet, and R. Mégy, Appl. Phys. Lett. **76**, 397 (2000).
[5] A. Cvitkovic, N. Ocelic, and R. Hillenbrand, Opt. Express **15**, 8550 (2007).
[6] T. Kalkbrenner, U. Håkanson, A. Schädle, S. Burger, C. Henkel, and V. Sandoghdar, Phys. Rev. Lett. **95**, 200801 (2005).
[7] J. Houel, S. Sauvage, P. Boucaud, A. Dazzi, R. Prazeres, F. Glotin, J.-M. Ortéga, A. Miard, and A. Lemaître, Phys. Rev. Lett. **99**, 217404 (2007).
[8] B. Kwon, M. V. Schulmerich, L. J. Elgass, R. Kong, S. E. Holton, R. Bhargava, and W. P. King, Ultramicroscopy **116**, 56 (2012).
[9] A. V. Shchegrov, K. Joulain, R. Carminati, and J.-J. Greffet, Phys. Rev. Lett. **85**, 1548 (2000).
[10] K. Joulain, J.-P. Mulet, F. Marquier, R. Carminati, and J.-J. Greffet, Surf. Sci. Rep. **57**, 59 (2005).
[11] Y. De Wilde, F. Formanek, R. Carminati, B. Gralak, P.-A. Lemoine, J.-P. Mulet, K. Joulain, Y. Chen, and J.-J. Greffet, Nature (London) **444**, 740 (2006).
[12] D. Polder and M. Van Hove, Phys. Rev. B **4**, 3303 (1971).
[13] J. P. Mulet, K. Joulain, R. Carminati, and J. J. Greffet, Microscale Therm. Eng. **6**, 209 (2002).
[14] S. Shen, A. Narayanaswamy, and G. Chen, Nano Lett. **9**, 2909 (2009).
[15] E. Rousseau, A. Siria, G. Jourdan, S. Volz, F. Comin, J. Chevrier, and J. J. Greffet, Nat. Photonics **3**, 514 (2009).
[16] R. S. Ottens, V. Quetschke, S. Wise, A. A. Alemi, R. Lundock, G. Mueller, D. H. Reitze, D. B. Tanner, and B. F. Whiting, Phys. Rev. Lett. **107**, 014301 (2011).
[17] R. S. Di Matteo, P. Greiff, S. L. Finberg, K. A. Young-Waithe, H. K. H. Choi, M. M. Masaki, and C. G. Fonstad, Appl. Phys. Lett. **79**, 1894 (2001).
[18] M. Laroche, R. Carminati, and J. J. Greffet, J. Appl. Phys. **100**, 063704 (2006).
[19] S. Basu, Z. M. Zhang, and C. J. Fu, Int. J. Energy Res. **33**, 1203 (2009).
[20] C. R. Otey, W. T. Lau, and S. Fan, Phys. Rev. Lett. **104**, 154301 (2010).
[21] A. C. Jones and M. B. Raschke, Nano Lett. **12**, 1475 (2012).
[22] K. Joulain, R. Carminati, J.-P. Mulet, and J.-J. Greffet, Phys. Rev. B **68**, 245405 (2003).
[23] K. H. Drexhage, Prog. Opt. **12**, 163 (1974).
[24] P. Anger, P. Bharadwaj, and L. Novotny, Phys. Rev. Lett. **96**, 113002 (2006).
[25] S. Kühn, U. Håkanson, L. Rogobete, and V. Sandoghdar, Phys. Rev. Lett. **97**, 017402 (2006).
[26] M. Frimmer, Y. Chen, and A. F. Koenderink, Phys. Rev. Lett. **107**, 123602 (2011).
[27] V. Krachmalnicoff, E. Castanié, Y. De Wilde, and R. Carminati, Phys. Rev. Lett. **105**, 183901 (2010).
[28] J.-J. Greffet, R. Carminati, K. Joulain, J.-P. Mulet, S. Mainguy, and Y. Chen, Nature (London) **416**, 61 (2002).
[29] F. Marquier, K. Joulain, J.-P. Mullet, R. Carminati, J.-J. Greffet, and Y. Chen, Phys. Rev. B **69**, 155412 (2004).
[30] Peter R. Griffiths and James A. De Haseth, *Fourier Transform Infrared Spectrometry* (John Wiley and Sons, Hoboken, New Jersey, 2007), 2nd ed.
[31] A. Bousseksou, A. Babuty, J-P. Tetienne, I. Moldovan-Doyen, R. Braive, G. Beaudoin, I. Sagnes, Y. De Wilde, and R. Colombelli, Opt. Express **20**, 13 738 (2012).
[32] See Supplemental Material at http://link.aps.org/supplemental/10.1103/PhysRevLett.110.146103 for movie and Figures.
[33] K. Joulain, P. Ben-Abdallah, P.-O. Chapuis, A. Babuty, and Y. De Wilde, arXiv:1201.4834.
[34] B. Knoll and F. Keilmann, Opt. Commun. **182**, 321 (2000).
[35] M. Schnell, A. Garcia-Etxarri, J. Alkorta, J. Aizpurua, and R. Hillenbrand, Nano Lett. **10**, 3524 (2010).
[36] V. Krachmalnicoff, D. Cao, A. Cazé, E. Castanié, R. Pierrat, N. Bardou, S. Collin, R. Carminati, and Y. De Wilde, arXiv:1301.2560.